DIAMOND AND RELATED MATERIALS

Available online at www.sciencedirect.com

SciVerse ScienceDirect

(This is a sample cover image for this issue. The actual cover is not yet available at this time.)

Tunable synthesis of carbon nanosheet/silicon nanowire hybrids for field emission applications

Shao-long Wu, Jian-hua Deng, Ting Zhang, Rui-ting Zheng, Guo-an Cheng *

Key Laboratory of Beam Technology and Material Modification of Ministry of Education, College of Nuclear Science and Technology, Beijing Normal University, Beijing 100875, P. R. China

ARTICLE INFO

ABSTRACT

Carbon nanosheets (CNSs) were synthesized on silicon nanowires (SiNWs) using microwave plasma enhanced chemical vapor deposition without any catalyst. The synthesized products are composed of graphene and graphite nanosheets, and the ratio of the two kinds of nanosheets depends on the growth conditions. The morphology of CNS/SiNW hybrids can be controlled by adjusting growth time, microwave power and carbon concentration. The field emission performances of the hybrids are greatly improved compared to that of the as-prepared SiNWs. The turn-on field at $10\ \mu A\ cm^{-2}$, applied field at $1\ mA\ cm^{-2}$ and field enhancement factor of the hybrids with optimal morphology are $3.0\ V\ \mu m^{-1}$, $4.2\ V\ \mu m^{-1}$ and 1612, respectively. The improvements of field emission properties are mainly attributed to the high-density separated CNSs with sharp edges.

© 2012 Elsevier B.V. All rights reserved.

1. Introduction

Since successfully isolated from bulk graphite by exfoliation techniques [1], graphene has attracted a great deal of interest [2]. Due to its novel electronic properties [3,4], graphene has potential applications in transparent electrodes [5], solar cells [6], gas sensors [7], transistors [8], spintronic devices [9], liquid crystal displays [10] and so on. Among these applications, the cold cathode field electron emitter is a prospective direction due to its large surface area, sharp edges and sustaining current densities [2,11]. However, the existing growth methods make graphene nanosheets or carbon nanosheets (CNSs) laying flat on substrate, which limits the field enhancement. There are some attempts, such as spin-coated graphene composite thin film [12], screen-printed graphene cathode [13], electrophoretic deposition of graphene films [14], and high temperature PECVD (plasma enhanced chemical vapor deposition) growth [15,16], to enhance the field emission (FE) via keeping the graphene nanosheets or CNSs stand on their edges. However, the FE properties of the CNSs prepared by these approaches are still limited due to the random orientation of CNSs. How to control the emitter density and avoid screening effect, which determine the field enhancement factor, are still great challenges.

Si nanowires (SiNWs) are regarded as promising field emitters due to the high aspect ratio, thermal stability and compatibility of modern semiconductor processes [17–19]. But their FE properties are inferior to that of carbon-based nanostructures, because the electronic properties of Si are worse than that of carbon. Therefore, various methods have been attempted to improve the FE properties of SiNWs, but these attempts usually bring a limited enhancement and some other undesired problems. Zhao et al. [20] decorated the as-grown SiNWs with Au particles, then carried out post-annealing to improve the FE properties, which was mainly contributed to the lower work function of Au-Si nanoparticle decorated SiNWs. Ultra-nano-crystalline diamond (UNCD) film was coated on SiNWs, and the applied field at $0.1\ mA\ cm^{-2}$ was reduced from $16\ V\ \mu m^{-1}$ for bare SiNWs to $10.2\ V\ \mu m^{-1}$ [21]. Compositing carbon nanotubes with SiNWs brought about low turn-on field (E_{to}) but poor current stability due to the tangled morphology of carbon nanotubes and week nanotube-SiNW adhesion [22]. The hybrids of 2D-CNSs and 1D-SiNWs have not been reported, but are expected to perform much better FE properties than the as-grown SiNWs and decorated SiNWs by other methods, if the CNSs with controllable density and sharp edges can be uniformly grown on the SiNWs.

In this paper, the CNS/SiNW hybrids were successfully synthesized via a two step method. First, SiNWs were obtained by a metal assisted chemical etching method. Second, the CNSs grew on the as-prepared SiNWs in a microwave (MW) PECVD system. The atomic layer number of nanosheets ranges from 2 to several dozens, implying that the CNSs consist of graphene nanosheets and graphite nanosheets. The hybrid morphology can be roughly controlled by adjusting growth conditions, and its influences on the FE characteristics were investigated systematically. The turn-on field at $10\ \mu A\ cm^{-2}$, applied field at $1\ mA\ cm^{-2}$ and field enhancement factor of the hybrids with optimized morphology are $3.0\ V\ \mu m^{-1}$, $4.2\ V\ \mu m^{-1}$ and ~1612, respectively, and the corresponding values of the as-prepared Si nanowires were $6.7\ V\ \mu m^{-1}$, $10.6\ V\ \mu m^{-1}$, and ~1202, respectively.

* Corresponding author. Tel./fax: +86 10 62205403.
  E-mail address: gacheng@bnu.edu.cn (G. Cheng).

2. Experimental details

2.1. Preparation of SiNWs

The SiNWs were prepared by metal assisted chemical etching of polished p-type Si (100, 25.5–42.5 Ωcm), similarly to our previous report [20]. The cut Si chips were ultrasonic cleaned in acetone, ethanol and de-ionized water for 10 min, respectively. Before the cleaned Si chips were used, they were immersed into the dilute HF for 2 min. To prepare SiNWs, the as-treated Si chips were dipped in the aqueous solution of 0.01 M $AgNO_3$ and 4.8 M HF for 1 min to deposit Ag nanoparticles (AgNPs). Sequently, the AgNPs-coated Si chips were diverted into the aqueous solution of 0.2 M H_2O_2 and 4.8 M HF for 40 min at room temperature. Finally, the chemical etched Si chips were soaked in 50% HNO_3 to remove the residual AgNPs, cleaned with de-ionized water and dried naturally in air for use.

2.2. Synthesis of CNSs on SiNWs

The uncatalyzed growth of CNSs was carried out in a vertically MW-PECVD system. Fig. 1 shows the conceptual schematic of MW-PECVD. The vacuum system consists of pipelines, valves, vacuum measurement instruments, mechanical and turbomolecular pumps. At the pressure of vacuum system negative of 1×10^{-3} Pa, H_2 flow of 50 sccm were introduced into the vacuum chamber. Then the sample stage, which was mobile and can be moved up and down by an electromotor, was heated up by a graphite heater attached to the stage holder. When the temperature reached 700 °C, MW started working. After the H plasma stabilized, C_2H_2 was introduced into the growth chamber. During the MW-PECVD growth process, the C_2H_2 and H_2 concentration, growth time, MW power, C_2H_2/H_2 ratio, and growth pressure were adjusted to study the influences of growth conditions on the morphology of hybrids.

2.3. Structural characterizations and FE measurements

The morphological and structural characterizations of the as-prepared SiNWs and hybrids were examined by a field emission scanning electron microscope (FE-SEM S-4800, Hitachi), a high resolution transmission electron microscope (HR-TEM JEM-2010, JEOL) and a Laser Resonance Raman spectroscopy with 633 nm excitation-wave (LobRAM, ARAMIS). FE measurements were carried out in a high vacuum chamber (~1×10^{-7} Pa) in a diode configuration at ~15 °C (cooled by water), the prepared samples worked as the cathode, and a stainless steel plate was adopted as the anode. The distance between cathode and anode was 600 μm. Voltage was applied from 0 to 10 kV, and the increasing rate was 300 Vmin^{-1}. The work function was determined by photoelectron spectrometer (AC-2, RIKEN KEIKI).

3. Results and discussion

The typical morphology of the as-prepared SiNWs is shown in Fig. 2(a)–(c). The NWs with diameters of 20–300 nm are uniform and perpendicular to the Si substrate. TEM image suggests that their surfaces are relative smooth and clean. Fig. 2(d)–(f) shows the typical morphology of the CNS/SiNW hybrids, which were synthesized in the 1:25 C_2H_2/H_2 volume ratio for 5 h, under MW power of 400 W at 2 kPa pressure. It can be observed that the curved CNSs are vertical to the surfaces of SiNWs. There are petal-like clusters of CNSs at the tips of SiNWs, but only separated CNSs on the lateral surfaces of SiNWs, suggesting the density of CNSs at the tips of SiNWs is larger than that on the lateral surfaces.

Various morphologies of CNS/SiNW hybrids and thicknesses of CNSs can be obtained under different growth conditions. Typical four different morphologies (labeled as sample A–D) were chosen to expound the influences of growth conditions on the morphology and the FE properties. As shown in Fig. 3, the CNS density of Sample A is much larger than that of Sample B, but the differences in the areas and thicknesses of CNS between Sample A and Sample B are
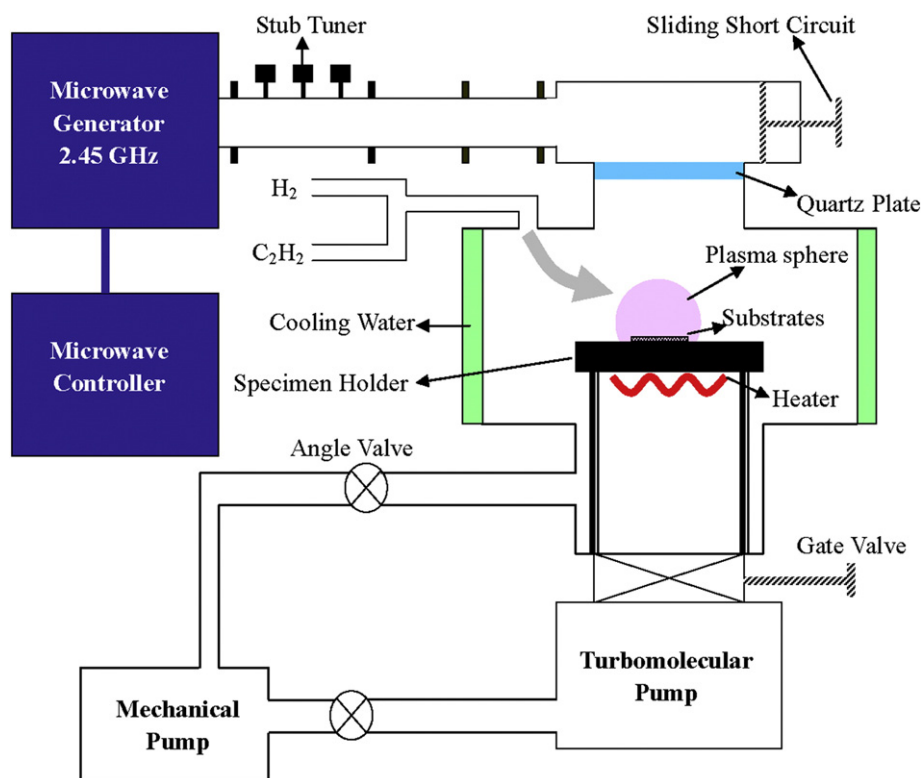

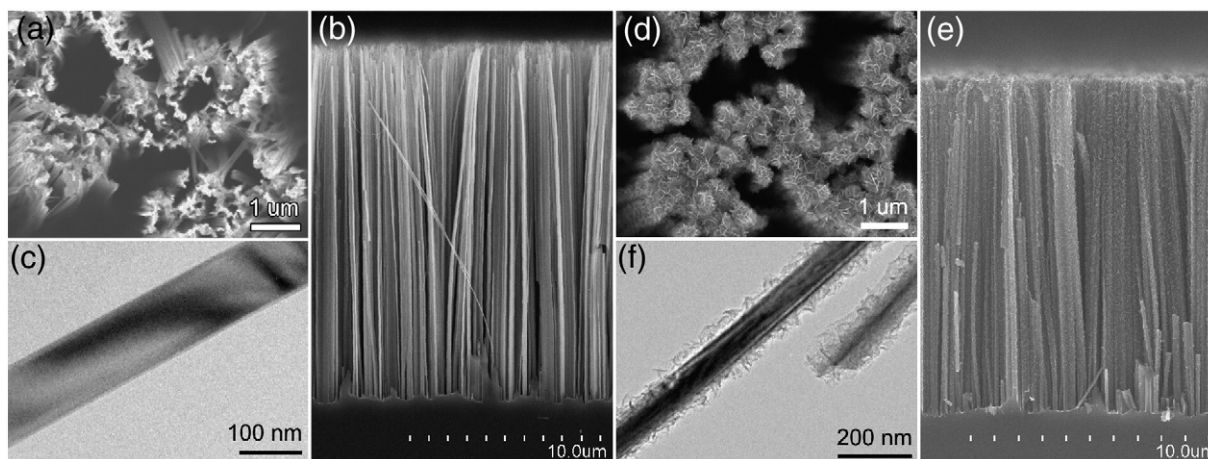**Fig. 1.** Conceptual scheme of the MW-PECVD system.

Fig. 2. Typical SEM and TEM images of the as-prepared SiNWs and CNS/SiNW hybrids. Top (a) and cross-sectional (b) view SEM images of the as-prepared SiNWs. (c) TEM image of the stripped SiNW. Top (d) and cross-sectional (e) view SEM images of the CNS/SiNW hybrids. (f) TEM image of CNSs grown on the stripped SiNW.

tiny. The high-density CNSs of Sample C and Sample D fill up the spacing between SiNWs. However, the CNS edges of sample C are sharper than that of sample A and sample B. The average CNS thicknesses of sample D are larger than that of sample A and sample B. The CNSs of sample C exhibit much sharper edges and larger areas than that of sample D. With comparison of the four different morphologies, it can be inferred that: 1) an increase of growth time results in a higher density of CNSs; 2) a higher MW power leads to a faster growth rate of CNS with sharper edges; 3) a lower C_2H_2 concentration makes uniform and thinner CNSs; 4) the appropriate growth conditions for isolated CNSs are growth time of 2–6 h, MW power between 200 and 800 W, and C_2H_2/H_2 flow ratio ranging from 1:30 to 1:20.

Besides the growth time, MW power and C_2H_2 concentration, the large surface-to-volume ratio and the excellent gas absorption ability of the as-prepared SiNWs also play a great role in the CNS growth. As a comparison, the cleaned planar Si was used as a substrate for

growing CNSs in the same MW-PECVD system. However, few CNSs were observed on the planar Si substrates under the same conditions. It mainly arises from the H plasma etching effect, defect-free surface and high surface potential of planar Si, which is unfavorable for carbon atom absorption and self-assembling. When the C_2H_2/H_2 ratio was increased from 1:25 to 2:5, there were sparse CNSs on the planar Si substrates after 3 h of growth. Moreover, the CNSs grown on planar Si substrates under harsh conditions show larger thicknesses than those grown on as-prepared SiNWs. The plasma was necessary in our synthesis process, and no CNSs were observed on the SiNWs without the plasma. Electric field induced by plasma promotes the growth at the nanosheet edges and makes their growth direction to be perpendicular to the substrate surfaces [23]. These results (more evidences are supplied in the Supplementary Material) suggest that the as-prepared SiNWs exhibit great advancements for PECVD growth of CNSs relative to the planar Si substrates.
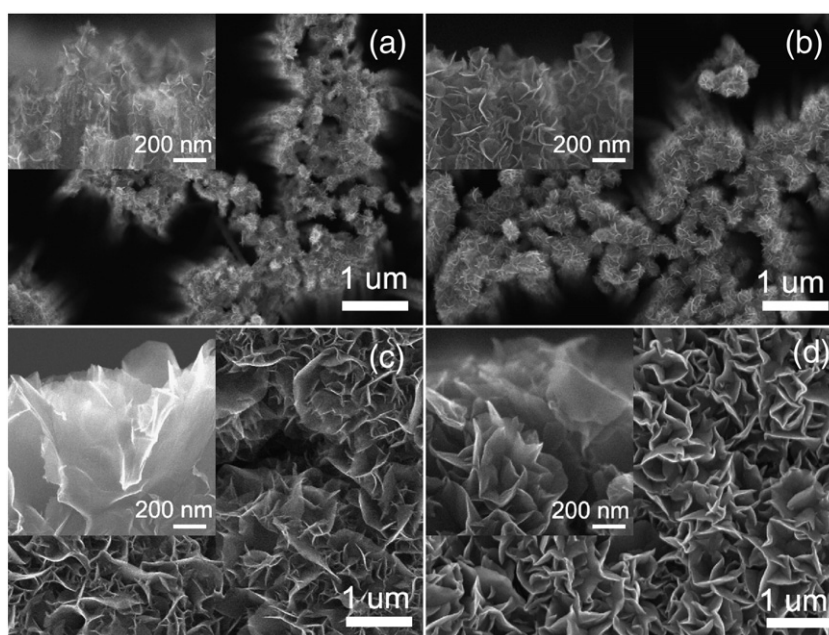

Fig. 3. Four typical different morphologies of hybrids. (a) Top view SEM image of sample A. Inset is cross-sectional view SEM image of the upper segment of sample A, which was fabricated under a 1:25 C_2H_2/H_2 volume for 1.5 h, under 400 W MW and 1.5 kPa gas pressure. (b) Top view SEM image of sample B. Inset is cross-sectional view SEM image of the upper segment of sample B, which was grown under a 1:25 C_2H_2/H_2 volume for 3 h, under 400 W MW and 1.5 kPa gas pressure. (c) Top view SEM image of sample C. Inset is cross-sectional view SEM image of the upper segment of sample C, which was prepared under a 1:25 C_2H_2/H_2 volume for 3 h, under 1200 W MW and 4.5 kPa gas pressure. (d) Top view SEM image of sample A. Inset is cross-sectional view SEM image of the upper segment of sample D, which was synthesized under a 1:5 C_2H_2/H_2 volume for 3 h, under 400 W MW and 1.5 kPa gas pressure.
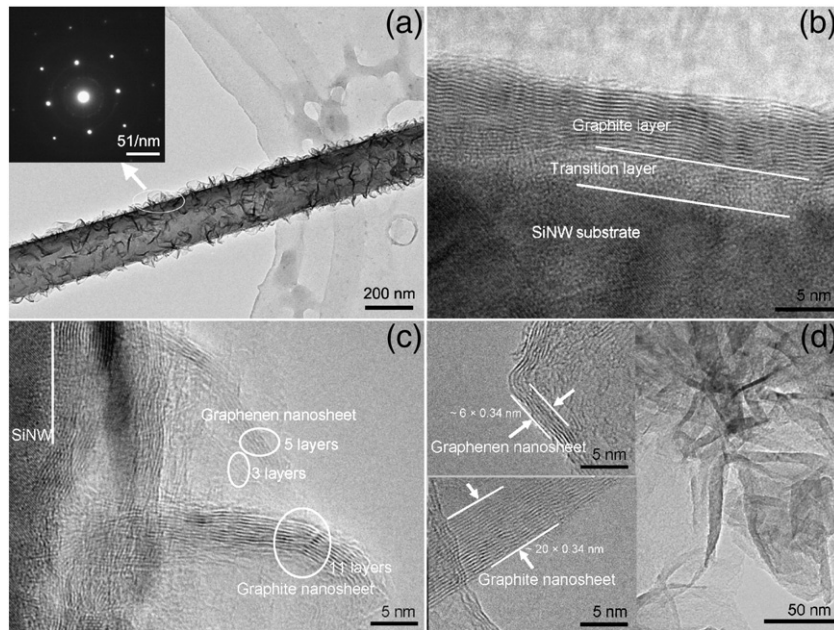
Fig. 4. TEM image analysis for CNS growth mechanism. (a) Low magnification image of CNSs grown on individual SiNWs. Inset is the SAED of region circled in (a). (b) High magnification image reveals that a graphite transition layer parallels to the surface of SiNW. (c) High magnification image suggests the upward curled edges of CNSs, which consist of graphene nanosheets and graphite nanosheets. (d) A cluster of CNSs at the tip of SiNWs. The top inset shows single graphene nanosheet determined by 6 atomic layers of the curled edge, and the bottom inset shows single graphite nanosheet determined by 20 atomic layers.

TEM image analysis of the CNSs grown on stripped SiNW reveals the details of CNS growth. Fig. 4(a) shows that the uniform CNSs are distributed on the profile-surfaces of SiNWs. Selective area electron diffraction (SAED) of CNS/SiNW hybrids is the combination effects of the disorder of CNSs, SiNW substrate, and transition layer between CNSs and SiNWs. Fig. 4(b) shows that a graphite layer parallels to the surface of SiNW, and the interlayer spacing is ~0.34 nm. There is a thin amorphous layer between Si substrate and graphite layer. Fig. 3(c) shows that the graphite layer is discontinuous and shows many irregular cracks over its entire surfaces, which may comes from the surface defect, internal stress, ion bombardment and lattice mismatch between the substrate and graphite [23]. The growth direction gradually turned into vertical to the surface as the graphite layer stretching at the cracks. The freestanding CNSs nucleate from these upward curled crack edges, grow up via accumulation and incorporation of carbon radical at the edges and sides. Meanwhile the H plasma is impinging the surfaces of the growing CNSs, and defects are removed by the etching effect [23,24]. Fig. 4(c) and (d) implies that the atomic layer number of CNSs ranges from 2 to several dozens, suggesting that the CNSs consist of graphene nanosheets and graphite nanosheets.

Fig. 5 shows the Raman spectra of the four forementioned samples; there are four distinct peaks centered at ~1333, ~1580, ~1615 and ~2650 cm^{-1}, corresponding to the D peak, G peak, D′ peak, and 2D peak, respectively. The appearance of the D peak is attributed to the defects or structural disorder of CNSs, including vacancies, non-uniformity, corrugation, and twisting, which is not observed for a perfect graphene sheet [25]. The G peak arises from E_{2g} vibration mode of all the sp^2 bonds of graphite [25,26]. The D′ peak is from the size effect in microcrystalline graphite, which is frequently observed in carbon nanomaterials [27]. The intensity ratio (R) of the D-to-G peaks can be applied to indicate the disorder degree of CNSs [28]. Our results indicate that the high crystalline structure of CNSs is obtained under high MW power and low C_2H_2 concentration with appropriate growth time. The most notable feature is the appearance of 2D peak, whose position and shape are demonstrated to be related to the formation and layer number of graphene nanosheets, and a broader and up-shifted 2D peak suggests that the graphene nanosheet has a

larger layer number and smaller intensity ratio ($R′$) of 2D-to-G peaks [25,26]. The $R′$ value of sample A is the largest, and that of sample D is the smallest, suggesting that the mean CNS thicknesses are the smallest for sample A, and the largest for sample D, which is consistent with the SEM and TEM observations. These results imply that few-layer graphene nanosheets were successfully synthesized, and the mean layer number is different under various growth conditions.

The CNS/SiNW hybrids have high-density nanosheets with atomic-scale edges, which are potential field electron emitters. Fig. 6 shows the current density (J) versus electric field (E) characteristics of the above four CNS/SiNW hybrids and as-prepared SiNWs. Comparing with the J–E curve of the as-prepared SiNWS, it can be observed that the hybrids obviously shift to the low electric field and have a stronger upward trend as electric field increasing. For samples A–D, the turn-on electric fields are 3.5, 3.0, 4.2, and 4.7 V μm^{-1}, respectively, and the applied fields (E_J) at a current
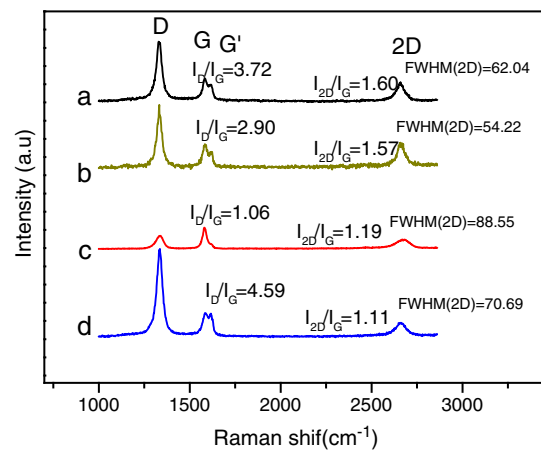

Fig. 5. Raman spectra of the four samples with different morphologies. I_D/I_G is the intensity ratio of D-to-G peaks, I_{2D}/I_G is the intensity ratio of 2D-to-G peaks, and FWHM (2D) is the full width at half maximum of 2D peaks. Curve a is the spectrum of Sample A, Curve b is the spectrum of Sample B, Curve c is the spectrum of Sample C, and Curve d is the spectrum of Sample D.
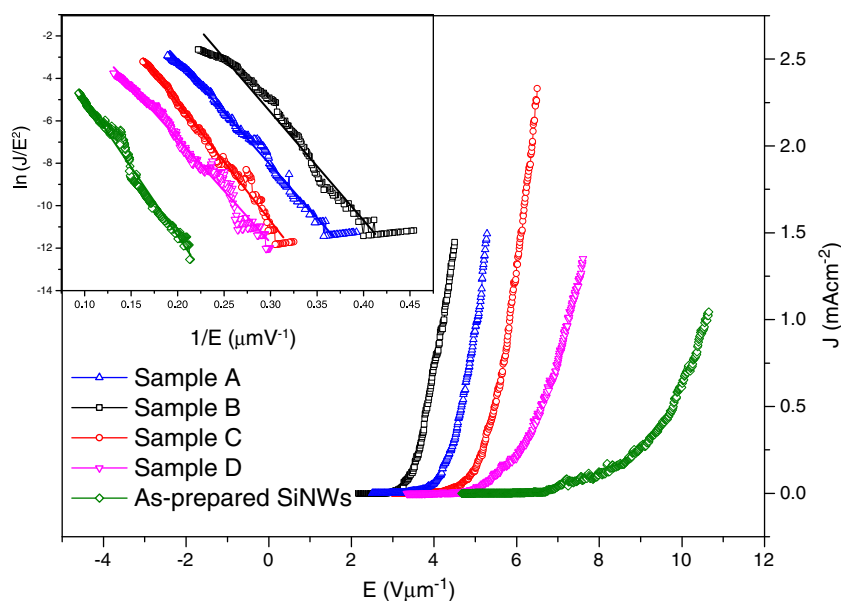
Fig. 6. Current density as a function of applied electric field of the four typical CNS/SiNW hybrids and as-prepared SiNWs. The inset is the corresponding F-N plots.

density of 1 mA cm^{-2} are 5.1, 4.2, 5.8 and 7.2 V μm^{-1}, respectively. Note that the FE properties of Sample B have a noticeable enhancement compared to that of sample A, owing to a higher density of CNSs in sample B. Sample D shows worse FE properties than sample C, mainly attributed to the larger thicknesses of CNSs in sample D. The observable maximum field emission current density is up to ~2.33 mA cm^{-2} for the hybrids at applied electric field of 6.5 V μm^{-1}, and the maximum current density is only ~1.04 mA cm^{-2} for the as-prepared SiNWs at applied electric field of 10.4 V μm^{-1}. Chen et al. [29] reported the CNSs grown on the planar Si and pyramidal Si(100) by a similar MW-PECVD method. The E_{to} values of CNSs grown on planar Si and pyramidal Si(100) were 4.6 and 3.2 V μm^{-1}, respectively, corresponding E_J values larger than 8.0 and 6.0 V μm^{-1}, respectively, which suggests that the CNS/SiNW hybrids have better FE properties than the as-prepared SiNWs and CNSs grown on planar Si or pyramidal Si(100).

To confirm the electron–emission mechanism and the difference in the field emission characteristics of various samples with different morphologies, we plotted $\ln(J/E^2)$ versus $1/E$ (as the inset in Fig. 6 shown). The good linearity of Fowler–Nordheim (F-N) plots suggest that these currents are indeed a result of the field electron emission. Due to the sharp edges of CNSs and high aspect ratios of SiNWs, dramatically enhanced local electric field is expected. The field enhancement factor (β) is calculated by $\beta = -B\phi^{3/2} m^{-1}$ from FN equation, where B is constant (6.83×10^9 V eV$^{-3/2}$ m^{-1}), ϕ is the

work function, and m is the slope of F-N plot [30–32]. The ϕ of samples A–D and as-prepared SiNWs are 4.62, 4.63, 4.59, 4.78 and 5.07 eV, respectively, determined by photoelectron spectrometer. And the corresponding β are ~1361, ~1612, ~1223, ~1459, and ~1202, respectively. The CNS/SiNW hybrids show a smaller ϕ value than the as-prepared SiNWs, suggesting the electron emission from the hybrids is more easily than from the as-prepared SiNWs. Samples A and B share the almost equal ϕ values, because the individual CNS of Samples A and B exhibits the identical thicknesses. Sample C has the smallest ϕ, owing to that the CNS edges are sharper than that of the other samples. Sample D synthesized under the highest C_2H_2 concentration shows the highest work function, attributed to the largest mean CNS thicknesses. As summarized in Table 1, the β values of the four hybrids are different, and the as-prepared SiNWs possess the smallest work function. It can be explained by the different densities and shapes of electron emitters. Combined effects of work function and field enhancement factor determine that the CNS/SiNW hybrids exhibit much better FE properties than the as-prepared SiNWs, and further enhancement is expected via optimizing morphology of SiNWs as well as CNS growth conditions.

4. Conclusions

CNS/SiNW hybrids were successfully fabricated by MW-PECVD. SiNWs were prepared in a simple metal assisted chemical etching method, and CNSs were directly synthesized on the as-prepared SiNWs. The morphology of CNS/SiNW hybrids can be controlled by adjusting growth time, MW power and C_2H_2 concentration. HRTEM and Raman analysis indicate that the CNSs consist of graphene nanosheets and graphite nanosheets. FE measurements demonstrate that the CNS/SiNW hybrids exhibit much better FE properties than the as-prepared SiNWs, and their morphology has great influences on the FE properties. The turn-on field at 10 μA cm^{-2}, the applied field at 1 mA cm^{-2}, and field enhanced factor of the hybrids with optimal morphology are 3.0 V μm^{-1}, 4.2 V μm^{-1}, and ~1612, respectively, and the corresponding values of the as-prepared SiNWs are 6.7 V μm^{-1}, 10.6 V μm^{-1}, and ~1202, respectively. These results demonstrate the CNS/SiNW hybrids are promising candidates for excellent field emitters, and also deserve more attention in other researches like energy harvest and storage.

Table 1
Field emission parameters of the four typical CNS/SiNW hybrids and as-prepared SiNWs.

Samples	$E_{J=10 \mu A\ cm^{-2}}$ (V μm^{-1})	$E_{J=1\ mA\ cm^{-2}}$ (V μm^{-1})	Φ (eV)	β
Sample A (1.5 h, 400 W, 1:25)	3.5	5.1	4.62	~1361
Sample B (3 h, 400 W, 1:25)	3.0	4.2	4.63	~1612
Sample C (3 h, 1200 W, 1:25)	4.2	5.8	4.59	~1223
Sample D (3 h, 400 W, 1:5)	4.7	7.2	4.78	~1459
As-prepared SiNWs	6.7	10.6	5.07	~1202

Acknowledgments

Appendix A. Supplementary data

Supplementary data to this article can be found online at doi:10. 1016/j.diamond.2012.05.001.

References

[1] K.S. Novoselov, A.K. Geim, S.V. Morozov, D. Jiang, Y. Zhang, S.V. Dubonos, I.V. Grigorieva, A.A. Firsov, Science 306 (2004) 666.
[2] A.K. Geim, Science 324 (2009) 1530.
[3] A.K. Geim, K.S. Novoselov, Nat. Mater. 6 (2007) 183.
[4] G. Eda, G. Fanchini, M. Chhowalla, Nat. Nanotechnol. 3 (2008) 270.
[5] T.J. Echtermeyer, M.C. Lemme, M. Baus, B.N. Szafranek, A.K. Geim, H. Kurz, IEEE Electron. Device Lett. 29 (2008) 952.
[6] S. Das, P. Sudhagar, V. Verma, D. Song, E. Ito, S.Y. Lee, Y.S. Kang, W. Choi, Adv. Funct. Mater. 31 (2011) 3729.
[7] F. Schedin, A.K. Geim, S.V. Morozov, E.W. Hill, P. Blake, M.I. Katsnelson, K.S. Novoselov, Nat. Mater. 6 (2007) 652.
[8] L. Liao, J. Bai, Y. Qu, Y. Huang, X. Duan, Nanotechnology 21 (2010) 015705.
[9] N. Tombros, C. Jozsa, M. Popinciuc, H.T. Jonkman, B.J. van Wees, Nature 448 (2007) 571.
[10] H.A. Becerill, J. Mao, Z. Liu, R.M. Stoltenberg, Z. Bao, Y. Chen, ACS Nano 2 (2008) 463.
[11] W.L. Wang, X.Z. Qin, N.S. Xu, Z.B. Li, J. Appl. Phys. 109 (2011) 044304.
[12] G. Eda, H.E. Unalan, N. Rupesinghe, G.A.J. Amaratunga, M. Chhowalla, Appl. Phys. Lett. 93 (2008) 233502.
[13] M. Qian, T. Feng, H. Ding, L.F. Lin, H.B. Li, Y.W. Chen, Z. Sun, Nanotechnology 20 (2009) 425702.
[14] Z.S. Wu, S.F. Pei, W.C. Ren, D.M. Tang, L.B. Gao, B.L. Liu, F. Li, L. Chang, H.M. Cheng, Adv. Mater. 21 (2009) 1756.
[15] J.J. Wang, M.Y. Zhu, R.A. Outlaw, X. Zhao, D.M. Manos, B.C. Holloway, V.P. Mammana, Appl. Phys. Lett. 85 (2004) 1265.
[16] W.C. Shih, J.M. Jeng, C.T. Huang, J.T. Lo, Vacuum 84 (2010) 1452.
[17] R. Riccitelli, A.D. Carlo, A. Fiori, S. Orlandcci, M.L. Terranova, A. Santoni, R. Fantoni, A. Rufoloni, F.J. Villacorta, J. Appl. Phys. 102 (2007) 054906.
[18] T.C. Cheng, J. Shieh, W.J. Huang, M.C. Yang, M.C. Cheng, H.M. Lin, M.N. Chang, Appl. Phys. Lett. 88 (2006) 263118.
[19] F. Zhao, D.D. Zhao, S.L. Wu, G.A. Cheng, R.T. Zheng, J. Korean Phys. Soc. 55 (2009) 2681.
[20] F. Zhao, G.A. Cheng, R.T. Zheng, D.D. Zhao, S.L. Wu, J.H. Deng, Nanoscale Res. Lett. 6 (2011) 176.
[21] Y.F. Tzeng, K.H. Liu, Y.C. Lee, S.J. Lin, I.N. Lin, C.Y. Lee, H.T. Chiu, Nanotechnology 18 (2007) 435703.
[22] Y.M. Liu, S.S. Fan, Solid State Commun. 133 (2005) 131.
[23] M. Zhu, J. Wang, B.C. Holloway, R.A. Outlaw, X. Zhao, K. Hou, V. Schutthanandan, D.M. Manos, Carbon 45 (2007) 2229.
[24] S.K. Srivastava, A.K. Shukla, V.D. Vankar, V. Kumar, Thin Solid Films 492 (2005) 124.
[25] A.C. Ferrari, J.C. Meyer, V. Scardaci, C. Casiraghi, M. Lazzeri, F. Piscanec, S. Mauri, D. Jiang, K.S. Novoselov, S. Roth, A.K. Geim, Phys. Rev. Lett. 97 (2006) 187401.
[26] C. Casiraghi, S. Pisana, K.S. Novoselov, A.K. Geim, A.C. Ferrari, Appl. Phys. Lett. 91 (2007) 233108.
[27] R.J. Nemanich, S.A. Solin, Phys. Rev. B 20 (1979) 392.
[28] G.D. Yuan, W.J. Zhang, Y. Yang, Y.B. Tang, Y.Q. Li, J.X. Wang, X.M. Meng, Z.B. He, C.M.L. Wu, I. Bello, C.S. Lee, S.T. Lee, Chem. Phys. Lett. 467 (2009) 361.
[29] Chen, C.M. Yeh, J.S. Syu, J. Hwang, C.S. Kou, Nanotechnology 18 (2007) 185706.
[30] Fowler, L. Nordheim, Proc. R. Soc. Lond. A 119 (1928) 173.
[31] Gadzuk, E.W. Plummer, Rev. Mod. Phys. 45 (1973) 487.
[32] Spridt, I. Brodie, L. Humphrey, E.R. Westerberg, J. Appl. Phys. 47 (1976) 5248.